Functional Electrical Stimulation by Nanogenerator with 58 V Output Voltage

ARTICLE *in* NANO LETTERS · MAY 2012

Impact Factor: 13.59 · DOI: 10.1021/nl300972f · Source: PubMed

NANO LETTERS

Letter

pubs.acs.org/NanoLett

Functional Electrical Stimulation by Nanogenerator with 58 V Output Voltage

Guang Zhu,[†] Aurelia C. Wang,[†] Ying Liu,[†] Yusheng Zhou,[†] and Zhong Lin Wang*[,†,‡]

[†]School of Materials Science and Engineering, Georgia Institute of Technology, Atlanta, Georgia 30332-0245, United States

[‡]Beijing Institute of Nanoenergy and Nanosystems, Chinese Academy of Sciences, Beijing, China

Supporting Information

ABSTRACT: We demonstrate a new type of integrated nanogenerator based on arrays of vertically aligned piezoelectric ZnO nanowires. The peak open-circuit voltage and short-circuit current reach a record high level of 58 V and 134 μA, respectively, with a maximum power density of 0.78 W/cm^3. The electric output was directly applied to a sciatic nerve of a frog, inducing innervation of the nerve. Vibrant contraction of the frog's gastrocnemius muscle is observed as a result of the instantaneous electric input from the nanogenerator.

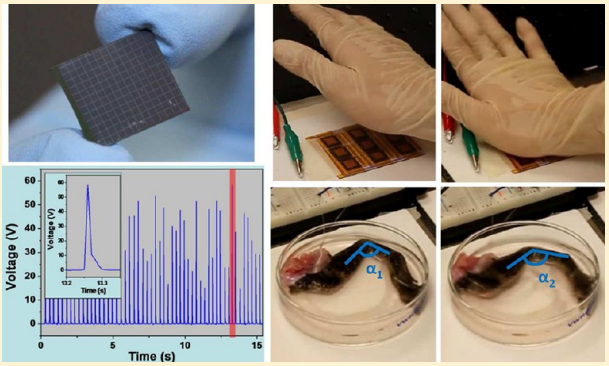

KEYWORDS: *Nanogenerator, ZnO, energy harvesting, functional electrical stimulation*

The modern life is inexorably dependent on emerging technologies in stand-alone portable systems designed to provide complete and personal solutions.[1] Integration of micro-to-nanosized sensors, actuators/transducers, and medical implants leads to ultraminiaturized and multifunctional smart systems that are expected to provide unprecedented life quality for human kinds.[2−4] For such a system that consumes much less power than do their bulky counterparts, it is not only significant but also very feasible to harvest ambient energy to build self-powered systems that can operate independently and sustainably. Here, we achieved real-time functional electrical stimulation (FES) of a sciatic nerve of a frog by a new type of ZnO-nanowire (NW)-based nanogenerator (NG) that produced electricity from biomechanical energy. The electric output from the NG reached a record high of 58 V and 134 μA, with a maximum power density of 0.78 W/cm^3. It was sufficient to directly and instantaneously induce innervating of the motor never and hence contraction of the frog's gastrocnemius muscle. Our demonstration suggests potential applications of the nanogenerator in biomedical and neurological fields, such as the power source for neuroprosthetic devices.

Since 2005, we have been developing "self-powered nanotechnology" by ZnO-nanowire-based NGs.[5,6] By virtue of the piezoelectric effect of ZnO NWs, the NGs target ambient mechanical energy, transforming it into electrical energy. As a result of worldwide efforts, such a concept is being developed into a practical technology with a variety of demonstrated applications.[7−13] However, a major limitation was that the output power of a NG was still not sufficiently high enough for real-time operation of conventional electronics.

The previously designed NGs utilized the Schottky barrier between metal−semiconductor contacts, which was required for charge accumulation.[5,14−16] In this work we developed a novel design and process flow for fabricating an integrated NG based on position-controlled vertical ZnO NWs. The Schottky contact was replaced by a thin insulating layer that prevents the current leakage through the internal structure. The process flow for fabrication is shown in Figure 1. A precleaned silicon substrate was consecutively deposited with an ITO layer and a ZnO seed layer by RF sputtering (Figure 1a−c). Not only does the ITO layer play a role as a conductive electrode, but also it promotes adhesion between the ZnO seed and the substrate. Photolithography was then performed to open an array of square windows on photoresist with narrow spacing in between (Figure 1d). The photoresist serves as a mask so that ZnO NWs only grow on the exposed seed surface in the subsequent synthesis step by wet mechical method (Figure 1e). Following stripping off any residual photoresist (Figure 1f), the NWs were thermally annealed. Then a layer of PMMA was applied cover the synthesized NWs (Figure 1g) by spin-coating, followed by depositing a top metal electrode of aluminum (Figure 1h). Finally, another layer of PMMA was used for packaging (Figure 1i). Two terminal leads rested on the ITO layer and the aluminum layer for electrical measurement. The process flow is compatible with batch fabrication techniques, which allow multiple silicon wafers to be parallel processed, followed by

Received: March 11, 2012
Revised: May 11, 2012

   dx.doi.org/10.1021/nl300972f | *Nano Lett.* XXXX, XXX, XXX−XXX

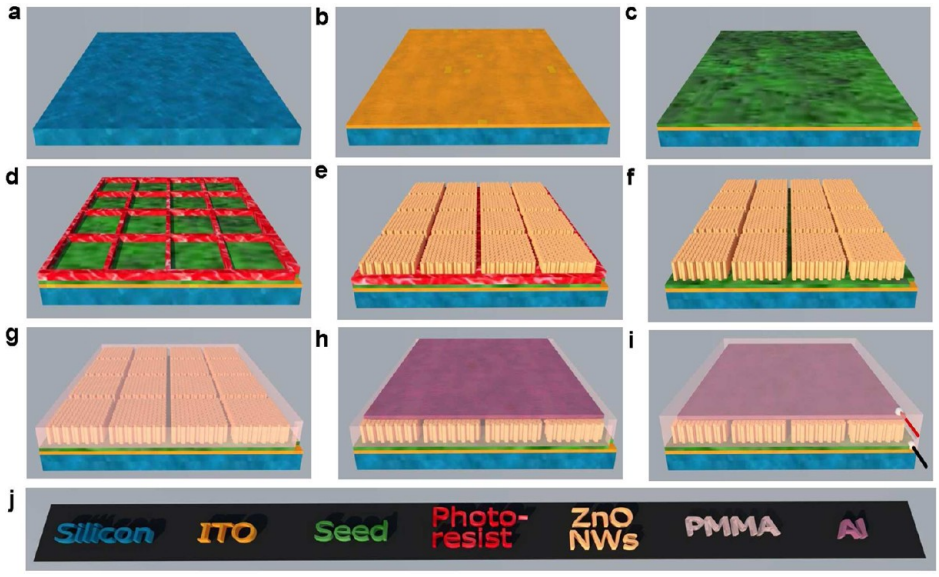

Figure 1. Process flow for fabricating the nanogenerator. (a) Silicon substrate. (b) Deposition of an ITO layer by sputtering. (c) Deposition of a ZnO seed layer by sputtering. (d) Window opening by photolithography. (e) Selective growth of ZnO NWs on the window areas by hydrothermal method. (f) Stripping off residual photoresist by acetone. (g) Spin-coating a PMMA layer to cover the structure. (h) Deposition of a metal layer as an electrode by e-beam evaporation. (i) Packaging by spin-coating another PMMA layer. (j) Legend of the figure.

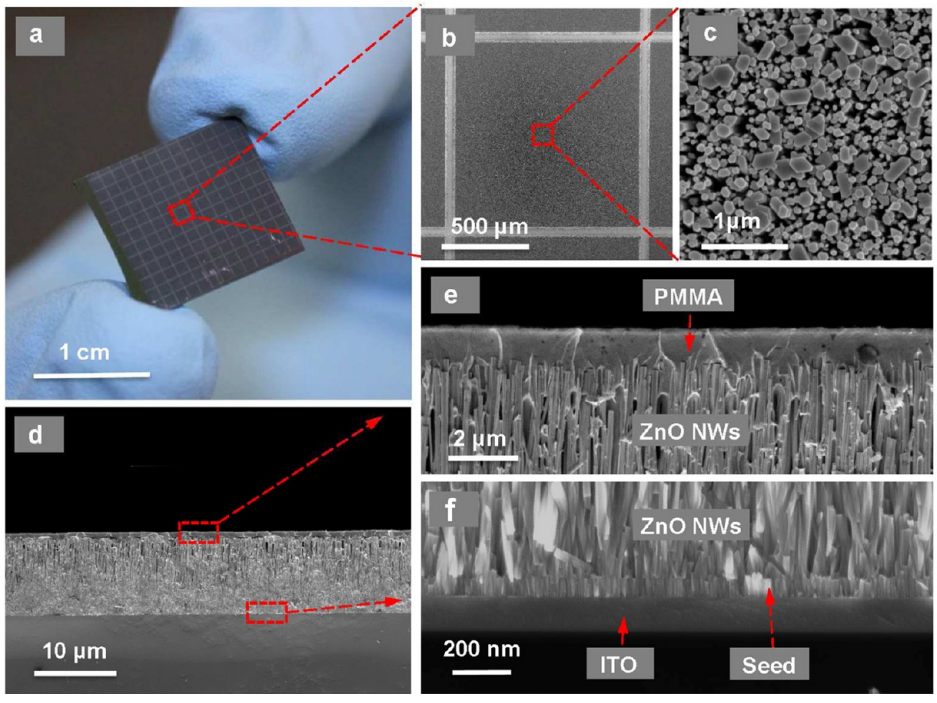

Figure 2. Structure of the nanogenerator. (a) Picture of the nanogenerator after position-controlled growth of ZnO NWs. (b) SEM image of one segment of the nanogenerator that is well-defined by photolithography. (c) SEM image of the synthesized ZnO NWs with a top view. (d) SEM image of the device structure after spin-coating a PMMA on the grown NWs with a cross-sectional view. (e) SEM that shows coverage of NWs by the PMMA layer. (f) SEM image of the seed layer and the ITO layer between NWs and the substrate.

being diced into individual devices. Therefore, it is superior in terms of production scale-up and cost reduction.

The result of the position-controlled synthesis is shown in Figure 2a. ZnO NWs grew only in designated areas defined by photolithography (Figure 2b). Such a design improves not only the effectiveness of NWs for energy harvesting but also the robustness of the NG for defect toleration because each unit can work independently. The high-magnification SEM image shows that the NWs are aligned vertically (Figure 2c). They are so densely grown that most of them are connected or even merged together (Figure 2d). The cross-sectional view of the structure (Figure 2e) reveals closely packed NWs that are submerged in PMMA.

The as-fabricated nanogenerator was mechanically triggered by a linear motor that provided dynamic impact with controlled force, speed, and frequency. A commercial bridge rectifier was

dx.doi.org/10.1021/nl300972f | *Nano Lett.* XXXX, XXX, XXX−XXX

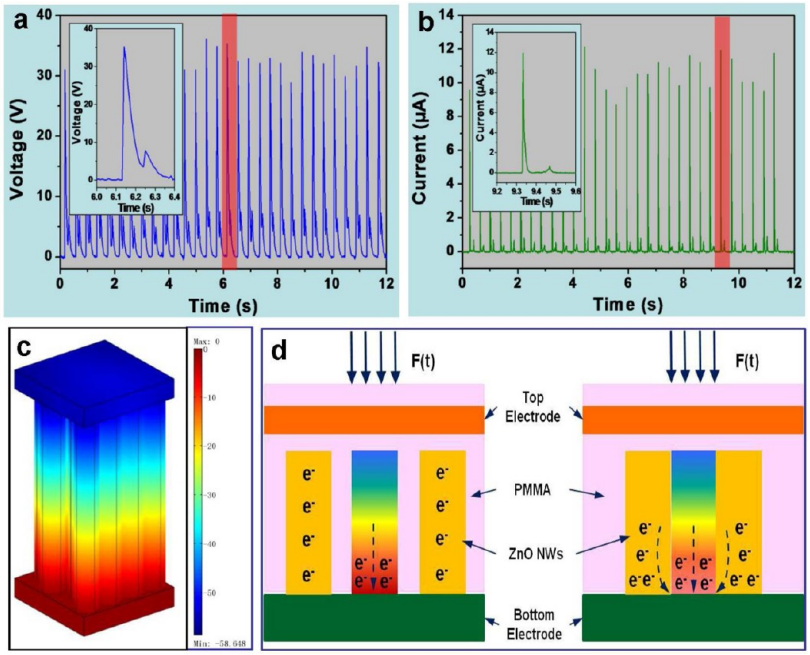

Figure 3. Performance characterization, simulation, and analysis of the nanogenerator. (a) Open-circuit voltage of the nanogenerator rectified by a bridge rectifier under a stress of 1 MPa and an enlarged view of one cycle in the shadowed region (inset). (b) Short-circuit current of the nanogenerator rectified by a bridge rectifier under a stress of 1×10^6 Pa and an enlarged view of one cycle in the shadowed region (inset). (c) Finite element calculation of the potential distribution across the nanogenerator under a stress of 1 MPa. (d) Analysis of the merit of the segmented design. The left-hand side schematic illustrates the case with segmentation, while the right-hand side one shows the case without segmentation (see text).

connected to the NG to convert the ac output into dc. For a NG with an effective dimension of 1 cm by 1 cm by 10 μm occupied by ZnO NWs, the open-circuit voltage (V_{oc}) and the short-circuit current (I_{sc}) reached up to 37 V (Figure 3a) and 12 μA (Figure 3b) under a stress of 1 MPa, respectively. The working mechanism of the NG can be described by the transient flow of inductive charges driven by the piezopotential. When the NG is subject to a compressive stress, a piezopotential field is created along the NWs. As a result of electrostatic force, inductive charges are established on the top and bottom electrodes, which are the flowing charges through an external load. In other words, the strained NWs are analogous to polarized dipole moments in a plate capacitor filled by a dielectric material. Once the stress is released, the disappearance of the piezopotential leads to back flow of the inductive charges through the load.[8,9]

The COMSOL package was used to carry out theoretical calculations of the piezopotential.[8,9,15] The calculated results predict an inductive potential difference of 45 V across the two electrodes at an applied stress of 1 MPa, as illustrated in Figure 3c. Reduced magnitude of the experimental result in comparison to the simulated value is probably due to the screening effect of the free carriers within the NWs.[17]

The superior performance and robustness of the newly designed NG are primarily attributed to the PMMA layer between the NWs and the metal electrode. Such a thin layer offers a number of advantages. First of all, it is an insulating layer that provides a potential barrier of infinite height, preventing the induced electrons in the electrodes from internal "leaking" through the ZnO/metal interface.[7,9,18] It replaces the Schottky contact in early designs. Furthermore, the PMMA fills the gap between NWs by capillary force and forms a capping at the very top. Consequently, when a force is applied along the vertical direction, the stress can be transmitted through the capping layer to all NWs under the force-applied area, greatly enhancing the NG's efficiency. This is a great improvement over some previous designs in which only a portion of NWs with proper length were in contact.[13,19,20] Furthermore, it serves as a buffer layer protecting NWs from intimate interaction with the electrode, improving the NG's robustness.[21]

It is also noteworthy that NWs were selectively grown in photolithography-designated regions. Such segmentation is designed to optimize the NG's output. Though thermal annealing during the fabrication might help reducing the concentration of free charge carriers,[22,23] there is still finite conductivity within ZnO NWs.[17] As a result, free charge carriers within the NWs will partially screen the piezopotential, leading to reduced magnitude of it and thus degraded performance of the NG. Shown by the cross-sectional image of the device in Figure 2d, the NWs are so densely packed that they are all electrically connected in parallel. On condition that a force is applied on an area smaller than the device's dimension or the applied force has a nonuniform distribution, only the NWs located directly beneath the force-applied area will experience strain and thus generate piezopotential (Figure 3d), which are referred to as active NWs. Owing to the presence of segmentation, native free charge carriers within the NWs that are not directly compressed under the force-applied area (referred to as inactive NWs) are isolated from the active NWs. Hence, they will not be involved in screening (left side of Figure 3d), preserving the piezopotential from further degradation. However, if no segmentation is made among the NWs, the free carriers in the inactive NWs tend to drift toward the high piezopotential side of the active NWs (right side of Figure 3d), which lower the local piezopotential and the thus the output.

dx.doi.org/10.1021/nl300972f | *Nano Lett.* XXXX, XXX, XXX−XXX

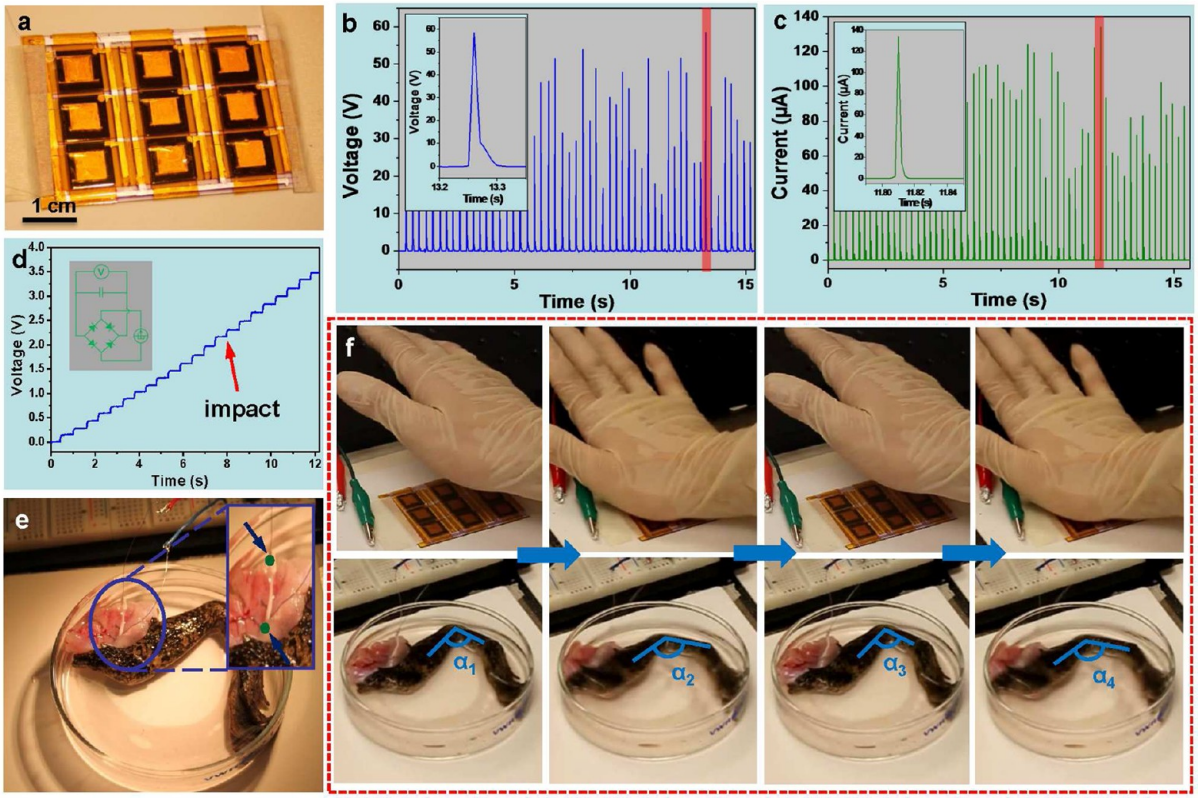

Figure 4. Nerve stimulation by the instantaneous output of nanogenerator. (a) Picture of the NG pad fabricated from nine nanogenerators connected in parallel. (b) Open-circuit voltage of the NG pad rectified by a bridge rectifier under impact by a human palm and an enlarged view of one cycle in the shadowed region (inset). (c) Short-circuit current of the NG pad rectified by a bridge rectifier under impact by a human palm and an enlarged view of one cycle in the shadowed region (inset). (d) Circuit diagram (inset) and voltage across a capacitor of 2 μF when being charged by the NG pad with every step corresponding to an impact. (e) Picture of a frog's hind limb with the sciatic nerve exposed and connected to the two terminals of the NG pad (inset). (f) Pictures that visualize real-time stimulation of the functional electrical stimulation by the NG pad. The leftmost pair and the second pair on the right correspond to intervals between impacts, with the gastrocnemius muscle at a standstill. The second pair on the left and the rightmost pair correspond to moments of impacts, with contraction of the gastrocnemius muscle. We use a α angle to characterize the instantaneous change in muscle shape as a result of the electric stimulation: α_1 equals α_3, while α_2 equals α_4.

The electric output can be tremendously scaled up by linear superposition. An energy-harvesting pad was fabricated with nine NGs in parallel connection (Figure 4a). Being punched by a human palm, the peak value of V_{oc} and I_{sc} exceeded 58 V and 134 μA, respectively (Figures 4b and 4c). Using such a significant output, we were able to charge a capacitor of 2 μF to over 3 V with less than 20 times of palm impact (Figure 4d).[20,24]

Using the instantaneous electric output of the NG pad for each palm impact, we successfully achieved real-time FES of a sciatic nerve of a frog. For a nerve cell at rest, it is normally polarized with a negative transmembrane potential.[25] At excitation, depolarization of the membrane is elicited by opening up voltage-gated ion channels. The cycle of depolarization and repolarization, also called the action potential, propagates through the nerve to activate motor tracts supplied to a muscle. As a consequence, muscle contraction is induced. Therefore, a voltage input equal to or greater than the threshold voltage above the resting potential would be required for firing of the action potential.[26] For a frog's sciatic nerve, the cells' resting potential ranges from −60 to −80 mV, and a voltage input of at least 50 mV at 1 Hz is necessary for innervation of the sciatic nerve.[25,27,28]

The NG pad was connected to an amputated hind limb of a frog by inserting the positive and negative terminals of the NG pad into the white corded sciatic nerve, as shown in Figure 4e. Throughout the experiment, the nerve was kept wet by Ringer's solution for amphibians. A human palm impacted the NG pad to generate electric impulses. Under the instantaneous electrical input, vibrant foot twitching was observed, resulting from contraction of the gastrocnemius muscle, as visualized in Figure 4f. The palm impact and foot twitching were perfectly synchronized (video in Supporting Information), indicating real-time stimulation using the electricity generated by each impact of a palm. Since the resistivity of the nerve soaked with Ringer's solution was very small, the actual voltage drop between the two terminal leads were expected to be much lower than the open-circuit voltage of the NG but still large enough to achieve FES.

In summary, using NGs based on ZnO NWs, we realized real-time FES of a sciatic nerve of a frog by converting biomechanical energy into electricity. The electric output from the NG reached a record high of 58 V and 134 μA, with a maximum power density of 0.78 W/cm^3, which is by far the highest output power ever achieved by piezoelectric NGs. We suggest that the nanogenerator might be applicable as a power source for neuroprosthetic devices, although considerable work will be necessary to realize such integration in the future.

dx.doi.org/10.1021/nl300972f | *Nano Lett.* XXXX, XXX, XXX−XXX

■ ASSOCIATED CONTENT

Supporting Information

Video of the functional electrical stimulation by the NG pad. This material is available free of charge via the Internet at http://pubs.acs.org.

■ AUTHOR INFORMATION

Corresponding Author

*E-mail: zlwang@gatech.edu.

Notes

The authors declare no competing financial interest.

■ ACKNOWLEDGMENTS

This research was supported by DARPA (HR0011-09-C-0142, Program manager, Dr. Daniel Wattendorf)), BES DOE (DE-FG02-07ER46394), and the Knowledge Innovation Program of Chinese Academy of Sciences (KJCX2-YW-M13).

■ REFERENCES

(1) Wang, Z. L. *Adv. Mater.* **2011**, *82*, 279.
(2) Wang, Z. L. *Sci. Am.* **2008**, *298*, 82.
(3) Patolsky, F.; Timko, B. P.; Yu, G.; Fang, Y.; Greytak, A. B.; Zheng, G.; Lieber, C. M. *Science* **2006**, *313*, 1100.
(4) Tian, B.; Cohen-Karni, T.; Qing, Q.; Duan, X.; Xie, P.; Lieber, C. M. *Science* **2010**, *329*, 831.
(5) Wang, Z. L.; Song, J. H. *Science* **2006**, *312*, 242.
(6) Xu, S.; Qin, Y.; Xu, C.; Wei, Y. G.; Yang, R. S.; Wang, Z. L. *Nat. Nanotechnol.* **2010**, *5*, 366.
(7) Zhu, G.; Yang, R.; Wang, S.; Wang, Z. L. *Nano Lett.* **2010**, *10*, 3151.
(8) Hu, Y.; Zhang, Y.; Xu, C.; Zhu, G.; Wang, Z. L. *Nano Lett.* **2010**, *10*, 5025.
(9) Hu, Y.; Zhang, Y.; Xu, C.; Lin, L.; Snyder, R. L.; Wang, Z. L. *Nano Lett.* **2011**, *11*, 2572.
(10) Hu, Y.; Lin, L.; Zhang, Y.; Wang, Z. L. *Adv. Mater.* **2012**, *24*, 110.
(11) Jung, J. H.; Lee, M.; Hong, J.; Ding, Y.; Chen, C.; Chou, L.; Wang, Z. L. *ACS Nano* **2011**, *5*, 10041.
(12) Kim, K.; Lee, K. K.; Seo, J.; Kumar, B.; Kim, S. *Small* **2011**, *7*, 2577.
(13) Chang, C.; Tran, V. H.; Wang, J.; Fuh, Y.; Lin, L. *Nano Lett.* **2010**, *10*, 726.
(14) Wang, X. D.; Song, J. H.; Liu, J.; Wang, Z. L. *Science* **2007**, *316*, 102.
(15) Gao, Y. F.; Wang, Z. L. *Nano Lett.* **2007**, *7*, 2499.
(16) Yang, R.; Qin, Y.; Dai, L.; Wang, Z. L. *Nat. Nanotechnol.* **2009**, *4*, 34−39.
(17) Gao, Y.; Wang, Z. L. *Nano Lett.* **2009**, *9*, 1103.
(18) Hu, Y.; Xu, C.; Zhang, Y.; Lin, L.; Snyder, R. L.; Wang, Z. L. *Adv. Mater.* **2011**, *23*, 4068.
(19) Xu, S.; Wei, Y. G.; Liu, J.; Yang, R.; Wang, Z. L. *Nano Lett.* **2008**, *8*, 4027.
(20) Xu, S.; Hansen, B. J.; Wang, Z. L. *Nat. Commun.* **2010**, *1*, xxxx.
(21) Periasamy, C.; Chakrabarti, P. *J. Appl. Phys.* **2011**, *109*, 054306.
(22) Pal, U.; Serrano, J. G.; Santiago, P.; Xiong, G.; Ucer, K. B.; Williams, R. T. *Opt. Mater.* **2006**, *29*, 65.
(23) Tam, K. H.; et al. *J. Phys. Chem. B* **2006**, *110*, 20865.
(24) Lee, M.; Bae, J.; Lee, J.; Lee, C.; Hong, S.; Wang, Z. L. *Energy Environ. Sci.* **2011**, *4*, 3359.
(25) Dodge, F. A.; Frankenhauser, B. *J. Physiol.* **1958**, *143*, 76.
(26) Raymond, S. A. *J. Physiol.* **1979**, *290*, 273.
(27) Frankenhauser, B. *J. Physiol.* **1957**, *135*, 550.
(28) Schalow, G.; Schmidt, H. *Pflugers Arch.* **1977**, *372*, 17.

■ NOTE ADDED AFTER ASAP PUBLICATION

This paper was published ASAP on May 18, 2012. The title of the paper has been updated. The revised version was posted on May 22, 2012.